The Efficiency of Excitation of a Surface Wave on a Dielectric Cylinder*

J. W. DUNCAN†

Summary—**This paper presents a theoretical and experimental study of the excitation of the lowest order TM surface wave on an infinite dielectric cylinder. The source is a circular filament of magnetic current within the dielectric rod. The integral solution for the field is evaluated as a contour integral by applying Cauchy's theorem. The far zone radiation field is obtained by means of a saddle point integration. Curves are presented which show excitation efficiency as a function of k_0a, the normalized circumferential length of the filament. A filament 0.83 wavelength in diameter will launch the TM mode with an efficiency of 95 per cent. A narrow annular slot in a large metal sheet was used to approximate the magnetic current filament and efficiency was measured using Deschamps' method for a two-port junction. The experimental measurements verify the theoretical analysis. In addition, it was found that the slot launching efficiency was essentially independent of the ground plane dimensions.**

Introduction

A NUMBER of papers published in the last decade have treated the mode characteristics of surface waves on various types of open waveguides. Of particular interest has been the utilization of such structures as surface wave antennas. A factor of prime importance in all surface wave applications is the efficient excitation of the desired mode on the guide. The excitation efficiency of a source is defined as the ratio of the power converted to the surface wave mode to the total power which is delivered by the source.

In order to determine the excitation efficiency of a source, one must solve the source form of Maxwell's equations which amounts to solving an inhomogeneous wave equation. The usual technique of solving the differential equation is to apply the method of integral transforms which yields the solution for the field in the form of a definite integral. The integral is evaluated by considering it as a contour integral in the plane of the complex propagation constant. The integrand has poles and branch points in the complex plane. Applying Cauchy's theorem to the contour integral, the integral becomes equal to the sum of the residues at the poles plus a branch cut integral. The poles correspond to the surface wave modes and the amplitude of a surface mode is given by the residue of the integrand at the pole. The branch cut integration yields the radiation field. Alternately, the radiation field is obtained from the asymptotic evaluation of the integral by means of a saddle point integration. This method of analysis yields the amplitude of the radiation field and of the surface mode. One may then calculate the radiated power and surface wave power and determine the excitation efficiency of the source.

Cullen[1] calculated the efficiency of an infinitely long slot above a dielectric coated plane conductor. He also treated the slot above a corrugated surface and a source such as a gently flared horn. His theory predicted a maximum efficiency of 85 per cent for the slot above the coated conductor. Rich[2] attempted an experimental verification of Cullen's work and measured efficiencies less than 20 per cent for the slot above the coated conductor. Several factors may have contributed to the difference in results.[3,4]

Fernando and Barlow[5] considered a vertical dipole source above flat reactive surfaces. A maximum efficiency of about 80 per cent was predicted for a half-wave dipole above a coated or a corrugated surface. In order to estimate efficiency experimentally, they measured the amplitude of the radiation and surface wave fields and substituted into the theoretical field solutions to calculate the respective powers and efficiency. Good agreement was obtained between the theoretical launching efficiency and the efficiency calculated from the measured amplitude of the fields.

Roberts[6,7] investigated the single wire transmission line excited from a flanged coaxial cable. This source launches the transverse magnetic, E_{00} mode on the wire. He evaluated the input conductance of the coaxial line by assuming an infinitesimal gap between the wire and the outer conductor of the coax. The input conductance is the sum of the radiation conductance G_1 and the characteristic conductance G_0. The excitation efficiency of the source may be calculated from G_1 and G_0. Roberts' experimental work included measuring the input conductance of the coaxial line for a number of different

* Manuscript received by the PGMTT, September 19, 1958. Revised manuscript received, December 3, 1958. The work described in this paper was supported by Wright Air Development Center under Contract No. AF33(616)-3220, and is extracted from a thesis submitted in partial fulfillment of the requirements for the Ph.D. degree, Dept. of Elec. Eng., University of Illinois, Urbana, Ill., 1958.

† Collins Radio Co., Cedar Rapids, Ia.

[1] A. L. Cullen, "The excitation of plane surface waves," *Proc. IEE*, vol. 101, pt. 4, pp. 225–234; August, 1954.

[2] G. J. Rich, "The launching of a plane surface wave," *Proc. IEE*, vol. 102, pt. B, pp. 237–246; March, 1955.

[3] A. L. Cullen, "Discussion on the launching of a plane surface wave," *Proc. IEE*, vol. 102, pt. B, pp. 824–825; November, 1955.

[4] R. H. DuHamel, "Discussion on the launching of a plane surface wave," *Proc. IEE*, vol. 103, pt. B, pp. 787–788; November, 1956.

[5] W. M. G. Fernando and H. E. M. Barlow, "An investigation of the properties of radial cylindrical surface waves launched over flat reactive surfaces," *Proc. IEE*, vol. 103, pt. B, pp. 307–318; May, 1956.

[6] T. E. Roberts, "Theory of the single wire transmission line," *J. Appl. Phys.*, vol. 24, pp. 57–67; January, 1953.

[7] T. E. Roberts, "An experimental investigation of the single wire transmission line," TRANS. IRE, vol. AP-2, pp. 46–56; April, 1954.

gap radii. The measured conductances were plotted on a graph and the curve was extrapolated to obtain the conductance of an infinitesimal gap, since it was impossible to measure such a source experimentally. The extrapolated value agreed quite closely with the conductance predicted from theory.

Most of the papers on excitation efficiency which have included experimental measurements have treated sources placed near infinite planar structures such as the dielectric coated conductor. Usually, it has not been feasible to measure efficiency for these structures. It seems worthwhile to apply the method of analysis to a problem which will permit direct experimental measurements of efficiency. The surface waveguide selected for the problem is the dielectric rod. The source, which has a simple physical realization, is the circular filament of magnetic current placed inside the rod and concentric with the longitudinal axis of the rod. One would expect the current ring to be an efficient exciter of the lowest order, transverse magnetic mode which can propagate on a dielectric rod. This mode is known as the E_{01} mode. The purpose of this investigation is to determine the efficiency with which the magnetic current ring excites the E_{01} mode and then to measure the efficiency experimentally. The excitation efficiency is readily measured using Deschamps' method for calibrating a two-port waveguide junction.

A similar problem has been treated by C. Jauquet,[8,9] who selected a magnetic current ring which was greater in diameter than the dielectric rod. In his papers, Jauquet obtains an integral solution for the field but does not present any calculations of excitation efficiency. His experimental measurements were concerned with the phase velocity and radial distribution of the surface wave mode.

Mathematical Formulation

The problem to be investigated is illustrated in Fig. 1.

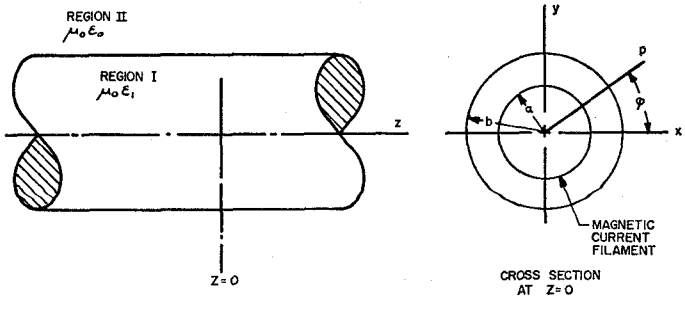

Fig. 1—Infinitely long dielectric rod excited by a circular filament of magnetic current located at $z=0$.

[8] C. Jauquet, "L'onde de surface sur un cylindre dielectrique le moyen de l'exciter—ses characteristiques," *Rev. HF*, vol. 3, no. 8, pp. 283–296; 1956.

[9] C. Jauquet, "Excitation d'une onde de surface transverse magnetique se propageant sur un cylindre dielectrique," *Ann. Telecommun.*, vol. 12, pp. 217–233; June, 1957.

An infinitely long, dielectric rod of radius b is located such that its longitudinal axis corresponds to the z axis of circular cylinder coordinates (ρ, ϕ, z). The rod is considered lossless, $\sigma=0$, with a magnetic permeability μ_0 and permittivity $\epsilon_1=\epsilon_r\epsilon_0$, where ϵ_r is the relative dielectric constant. The medium surrounding the rod and extending to infinity is free space, with constants μ_0 and ϵ_0. The electromagnetic field source is a filamentary ring of magnetic current located at the plane $z=0$. The ring is of radius a, where $0<a<b$, and is infinitesimally small in cross section. The source distribution is represented as a product of Dirac delta functions in the ρ and z coordinates as follows:

$$\overline{K} = \bar{\phi}\delta(\rho - a)\delta(z) \tag{1}$$

where $\bar{\phi}$ is a unit vector in the ϕ direction. The source distribution $\overline{K}$ is independent of ϕ and is a unit source such that

$$\iint \overline{K}\cdot\bar{\phi}da = \int_{a-\Delta}^{a+\Delta}\int_{0-\Delta}^{0+\Delta}\delta(\rho - a)\delta(z)dzd\rho = 1.$$

$\overline{K}$ has the dimensions of volts per square meter.

The electromagnetic field is a solution of Maxwell's equations. Written in differential form for $e^{-i\omega t}$ time dependence, we have

$$\begin{aligned}\nabla\times\overline{E} &= i\omega\mu\overline{H} - \overline{K}\\ \nabla\times\overline{H} &= -i\omega\epsilon\overline{E}.\end{aligned} \tag{2}$$

Taking the curl of the second equation and then substituting the first relation for $\nabla\times\overline{E}$ yields

$$-\nabla\times\nabla\times\overline{H} + \omega^2\mu\epsilon\overline{H} = -i\omega\epsilon\overline{K}. \tag{3}$$

The only non-zero component of $\overline{K}$ is the coefficient of the unit vector $\bar{\phi}$. We may write the ϕ component of the vector equation (3) and obtain the nonhomogeneous scalar equation

$$(-\nabla\times\nabla\times\overline{H}]_\phi + \omega^2\mu\epsilon H_\phi = -i\omega\epsilon\delta(\rho - a)\delta(z)$$

where the $\bar{\phi}$ component of the bracketed term is indicated.

The magnetic current filament generates a field having components H_ϕ, E_ρ, and E_z, while the components E_ϕ, H_ρ, and H_z are equal to zero. Due to the symmetry of the source, the field is independent of ϕ and we note that all partial derivatives with respect to ϕ must be zero. It is evident that the source produces a field which is circularly symmetric and transverse magnetic with respect to the z axis. Expanding the bracketed term in cylindrical coordinates, we obtain the partial differential equation relating $H_\phi(\rho, z)$ to the source

$$\frac{\partial^2 H_\phi}{\partial\rho^2} + \frac{1}{\rho}\frac{\partial H_\phi}{\partial\rho} + \left(k^2 - \frac{1}{\rho^2}\right)H_\phi + \frac{\partial^2 H_\phi}{\partial z^2} = -i\omega\epsilon\delta(\rho - a)\delta(z) \tag{4}$$

where $k^2=\omega^2\mu\epsilon$.

From $\overline{E}=(1/-i\omega\epsilon)\nabla\times\overline{H}$, it follows that

$$E_\rho(\rho, z) = \frac{1}{i\omega\epsilon}\frac{\partial H_\phi}{\partial z}$$

$$E_z(\rho, z) = \frac{1}{-i\omega\epsilon}\left(\frac{\partial H_\phi}{\partial \rho}+\frac{1}{\rho}H_\phi\right). \quad (5)$$

In order to solve (4) for H_ϕ, we shall apply the method of integral transforms to reduce (4) to a nonhomogeneous, ordinary differential equation. We define the Fourier transform of $H_\phi(\rho, z)$ as

$$h(\rho, \zeta) = \int_{-\infty}^{+\infty} H_\phi(\rho, z)e^{-i\zeta z}dz. \quad (6)$$

The inverse transform is given by

$$H_\phi(\rho, z) = \frac{1}{2\pi}\int_{-\infty}^{+\infty} h(\rho, \zeta)e^{i\zeta z}d\zeta. \quad (7)$$

Assuming that the transform of $H_\phi(\rho, z)$ exists, we multiply each term of (4) by $e^{-i\zeta z}$ and integrate over the infinite range with respect to z to obtain

$$\frac{d^2h}{d\rho^2}+\frac{1}{\rho}\frac{dh}{d\rho}+\left(k^2-\zeta^2-\frac{1}{\rho^2}\right)h = -i\omega\epsilon\delta(\rho-a) \quad (8)$$

where the source variation $\delta(z)$ is no longer present since

$$\int_{-\infty}^{+\infty}\delta(z)e^{-i\zeta z}dz = 1.$$

We may consider (8) as an ordinary differential equation in which ζ is a parameter constant. The boundary conditions on $h(\rho, \zeta)$ are obtained by taking the Fourier transform of the original boundary conditions on $H_\phi(\rho, z)$ and $\partial H_\phi/\partial\rho$. The problem is one of solving (8) for $h(\rho, \zeta)$ subject to the transformed boundary conditions. $H_\phi(\rho, z)$ is then obtained by use of the inverse transform (7). The integral expression for $H_\phi(\rho, z)$ is derived in the following section.

Solution of the Boundary Value Problem

Consider the form of the nonhomogeneous differential (8). One could solve (8) using the Hankel transform; however, the definition of the delta function allows one to solve (8) in a simpler manner. The delta function is defined by the relations

$$\int_{a-\Delta}^{a+\Delta}\delta(\rho-a)d\rho = 1, \text{ and } \delta(\rho-a) = 0 \text{ for } \rho \neq a.$$

Consequently, for all ρ other than $\rho=a$, (8) reduces to the homogeneous differential equation

$$\frac{d^2h}{d\rho^2}+\frac{1}{\rho}\frac{dh}{d\rho}+\left(k^2-\zeta^2-\frac{1}{\rho^2}\right)h = 0. \quad (9)$$

The delta function $\delta(\rho-a)$ implies a boundary condition which $h(\rho, \zeta)$ must satisfy at $\rho=a$. Multiplying each term of (8) by $d\rho$ and integrating over the interval 2Δ from $\rho=a-\Delta$ to $\rho=a+\Delta$, one obtains

$$\frac{dh}{d\rho}\Big|_{a-\Delta}^{a+\Delta}+\int\frac{1}{\rho}\left(\frac{dh}{d\rho}\right)d\rho+(k^2-\zeta^2)\int h d\rho$$

$$+\frac{1}{\rho}h\Big|_{a-\Delta}^{a+\Delta}-\int\frac{1}{\rho}\left(\frac{dh}{d\rho}\right)d\rho = -i\omega\epsilon\int_{a-\Delta}^{a+\Delta}\delta(\rho-a)d\rho. \quad (10)$$

Assuming that $h(\rho, \zeta)$ is continuous for all ρ, in the limit as $\Delta\to 0$ and $\rho\to a$, (10) reduces to

$$\frac{dh}{d\rho}\Big|_{a+\Delta}-\frac{dh}{d\rho}\Big|_{a-\Delta} = -i\omega\epsilon. \quad (11)$$

We have shown that a continuous $h(\rho, \zeta)$ which satisfies the homogeneous equation (9) and whose first derivative is discontinuous by $-i\omega\epsilon$ at $\rho=a$ is a solution of (8).

The remaining boundary conditions on $h(\rho, \zeta)$ follow from the boundary conditions imposed on $H_\phi(\rho, z)$ and $E_z(\rho, z)$ by Maxwell's equations. Referring to Fig. 1, we denote the cross-sectional area of the rod as region I and the space outside the rod as region II. Since tangential $\overline{H}$ is continuous at a magnetic current discontinuity, we see that $H_\phi(\rho, z)$ is continuous at $\rho=a$ for all z including the filament position $z=0$. Since tangential $\overline{E}$ and $\overline{H}$ are continuous across a dielectric boundary, we note that $H_\phi(\rho, z)$ and $E_z(\rho, z)$ must be continuous at $\rho=b$ for all z. The corresponding conditions on $h(\rho, \zeta)$ are

1) $H_\phi(\rho, z)$ continuous at $\rho=a$ for all z implies that

$$h(\rho, \zeta) = \int_{-\infty}^{+\infty} H_\phi(\rho, z)e^{-i\zeta z}dz$$

must also be continuous at $\rho=a$, hence

$$h(\rho, \zeta)\big|_{a-\Delta} = h(\rho, \zeta)\big|_{a+\Delta}. \quad (12)$$

2) Similarly, since $H_\phi(\rho, z)$ is continuous at $\rho=b$ for all z,

$$h(\rho, \zeta)\big|_{b-\Delta} = h(\rho, \zeta)\big|_{b+\Delta}. \quad (13)$$

3) From (5) we write

$$E_z(\rho, z) = \frac{1}{-i\omega\epsilon}\left(\frac{\partial H_\phi}{\partial\rho}+\frac{1}{\rho}H_\phi\right).$$

In region I, where $0\leq\rho\leq b$, the permittivity $\epsilon_1=\epsilon_r\epsilon_0$. In region II, where $\rho>b$, $\epsilon=\epsilon_0$. $E_z(\rho, z)$ continuous at $\rho=b$ for all z requires

$$\frac{\partial H_\phi}{\partial\rho}+\frac{1}{\rho}H_\phi\Big|_{b-\Delta} = \epsilon_r\left(\frac{\partial H_\phi}{\partial\rho}+\frac{1}{\rho}H_\phi\right)\Big|_{b+\Delta}.$$

Taking the transform, we obtain

$$\epsilon_r\frac{dh}{d\rho}\Big|_{b+\Delta}-\frac{dh}{d\rho}\Big|_{b-\Delta}+(\epsilon_r-1)\frac{1}{\rho}h\Big|_{b+\Delta} = 0 \quad (14)$$

by reason of (13).

In order to determine $H_\phi(\rho, z)$ in region II, we must solve (8) for the corresponding $h(\rho, \zeta)$. Inside the dielectric rod, for all ρ except $\rho=a$, (8) becomes

$$\frac{d^2h}{d\rho^2}+\frac{1}{\rho}\frac{dh}{d\rho}+\left(k_1^2-\zeta^2-\frac{1}{\rho^2}\right)h=0 \qquad (15)$$

where $k_1^2=\omega^2\mu_0\epsilon_1$. Outside the dielectric rod and for all ρ, (8) becomes

$$\frac{d^2h}{d\rho^2}+\frac{1}{\rho}\frac{dh}{d\rho}+\left(k_0^2-\zeta^2-\frac{1}{\rho^2}\right)h=0 \qquad (16)$$

where $k_0^2=\omega^2\mu_0\epsilon_0$.

We proceed by writing general solutions $h(\rho, \zeta)$ of (15) for the regions $0\leq\rho\leq a$, and $a\leq\rho\leq b$. The discontinuity at $\rho=a$ appears in the boundary condition (11). A general solution of (16) yields $h(\rho, \zeta)$ for the region $\rho\geq b$. The three solutions possess six arbitrary constants. The constants are determined from the requirements that the field be finite at $\rho=0$, that the field be regular at infinity and that it satisfy the radiation condition, and the four boundary conditions (11), (12), (13), and (14). Choosing the solution $h(\rho, \zeta)$ for region II, the inverse transform (7) must then be evaluated to yield $H_\phi(\rho, z)$ for $\rho\geq b$.

Eq. (15) is recognized as a form of Bessel's differential equation. It has the general solution

$$h(\rho, \zeta) = AJ_1(\nu_1\rho) + PY_1(\nu_1\rho)$$

where A and P are arbitrary constants, $J_1(\nu_1\rho)$ and $Y_1(\nu_1\rho)$ are Bessel functions of the first and second kind, respectively, and

$$\nu_1^2 = k_1^2 - \zeta^2.$$

Consider the region $0\leq\rho\leq a$. Since $H_\phi(\rho, z)$ and, therefore, $h(\rho, \zeta)$ must be finite at $\rho=0$, we determine that $P=0$, since $Y_1(\nu_1\rho)$ is unbounded as $\rho\to 0$. Hence,

$$h(\rho, \zeta) = AJ_1(\nu_1\rho) \qquad (17)$$

where

$$\nu_1 = \sqrt{k_1^2 - \zeta^2}$$
$$0 \leq \rho \leq a.$$

For the region $a\leq\rho\leq b$, the Y_1 function must be included, and we have

$$h(\rho, \zeta) = BJ_1(\nu_1\rho) + CY_1(\nu_1)\rho. \qquad (18)$$

A general solution of (16) is written in terms of Hankel functions of the first and second kind

$$h(\rho, \zeta) = DH_1^{(1)}(\nu_0\rho) + QH_1^{(2)}(\nu_0\rho)$$

where

$$\nu_0 = \sqrt{k_0^2 - \zeta^2}.$$

It will be seen later that, in general, ν_0 is complex; therefore we define the argument of ν_0 to be $0\leq\arg\nu_0\leq\pi$. As $\rho\to\infty$, $H_1^{(1)}(\nu_0\rho)$ vanishes and $H_1^{(2)}(\nu_0\rho)$ is unbounded for the defined argument of ν_0; therefore, $Q=0$ and we obtain

$$h(\rho, \zeta) = DH_1^{(1)}(\nu_0\rho) \qquad (19)$$

where

$$\nu_0 = \sqrt{k_0^2 - \zeta^2}; \qquad \begin{matrix} 0 \leq \arg\nu_0 \leq \pi \\ \rho \geq b \end{matrix}.$$

In order to solve for the arbitrary constants A, B, C, and D, we apply the boundary conditions (11), (12), (13), and (14) to the appropriate solutions (17), (18), and (19). Omitting the details, the following four equations are obtained:

$$-(\nu_1 b)AJ_1'(\nu_1 a) + (\nu_1 b)BJ_1'(\nu_1 a) + (\nu_1 b)CY_1'(\nu_1 a) = -i\omega\epsilon_1 b$$

$$AJ_1(\nu_1 a) - BJ_1(\nu_1 a) - CY_1(\nu_1 a) = 0$$

$$BJ_1(\nu_1 b) + CY_1(\nu_1 b) - DH_1^{(1)}(\nu_0 b) = 0$$

$$(\nu_1 b)BJ_1'(\nu_1 b) + (\nu_1 b)CY_1'(\nu_1 b) - D[\epsilon_r(\nu_0 b)H_1'^{(1)}(\nu_0 b) + (\epsilon_r - 1)H_1^{(1)}(\nu_0 b)] = 0. \qquad (20)$$

This system of equations was solved by finding the inverse of the coefficient matrix. The constant D was determined to be

$$D = i\omega\epsilon_1 a \frac{J_1(\nu_1 a)}{(\nu_1 b)J_0(\nu_1 b)H_1^{(1)}(\nu_0 b) - \epsilon_r(\nu_0 b)J_1(\nu_1 b)H_0^{(1)}(\nu_0 b)}. \qquad (21)$$

Substituting (21) into (19) we obtain $h(\rho, \zeta)$ for the region $\rho\geq b$. The solution $h(\rho, \zeta)$ is then substituted into the inverse transform (7) to yield the integral expression for $H_\phi(\rho, z)$ in region II. This result is

$$H_\phi(\rho, z) = \frac{i\omega\epsilon_1 a}{2\pi} \cdot \int_{-\infty}^{+\infty} \frac{J_1(\nu_1 a)H_1^{(1)}(\nu_0\rho)e^{i\zeta z}d\zeta}{(\nu_1 b)J_0(\nu_1 b)H_1^{(1)}(\nu_0 b) - \epsilon_r(\nu_0 b)J_1(\nu_1 b)H_0^{(1)}(\nu_0 b)} \qquad (22)$$

where

$$\nu_1 = \sqrt{k_1^2 - \zeta^2}; \qquad \nu_0 = \sqrt{k_0^2 - \zeta^2}$$

and

$$\rho \geq b.$$

Singularities of the Integrand—Solution of the Mode Equation

We wish to evaluate the real infinite integral (22). This is accomplished by considering it as a contour integral in the complex ζ plane and applying Cauchy's residue theorem. The path of closure in the complex plane is selected to ensure convergence of the integral. Evaluation of the contour integral is treated in the following section. For the present we shall consider ζ complex and determine the singularities of the integrand of (22).

Branch Points

Consider the variable ν_1 which appears in the arguments of J_0 and J_1 in (22). Since $\nu_1=\sqrt{k_1^2-\zeta^2}$, then ν_1 is multiple-valued in any neighborhood of $\zeta=\pm k_1$. However, if one considers the power series expansions of J_0 and J_1, one sees that the integrand is an even function of ν_1 so that the points $\zeta=\pm k_1$ are not actually branch points. The Hankel function arguments contain the variable $\nu_0=\sqrt{k_0^2-\zeta^2}$. The Hankel function has a logarithmic singularity at $\nu_0=0$, and so is multiple-valued in any neighborhood of $\zeta=\pm k_0$. The points $\pm k_0$ are, therefore, branch points of the integrand. We select branch cuts in the ζ plane as shown in Fig. 2. We note that $k^2=\omega^2\mu\epsilon$ is real. Thus, the points $\pm k_1$ and the $\pm k_0$ lie on the real axis with $|k_1|>|k_0|$ since $\epsilon_1>\epsilon_0$. The branch cuts are defined as $\zeta=\pm k_0+i$ Im ζ.

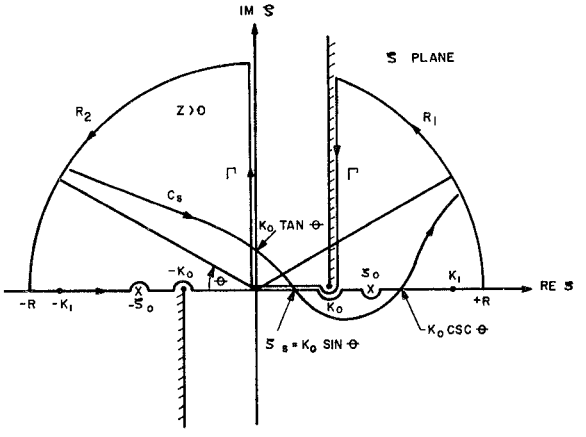

Fig. 2—Contour of integration in the ζ plane.

Poles

Before we investigate the integrand of (22) for poles, we shall discuss the significance of a pole in the physical problem. Assume that the point $\zeta=\zeta_0$ is a pole of the integrand. When (22) is evaluated as a contour integral, a residue contribution at ζ_0 must be included. Thus, $H_\phi(\rho, z)$ will have a term of the form

$$AH_1^{(1)}(\nu_0\rho)e^{i\zeta_0 z}. \tag{23}$$

Since we assumed a lossless dielectric rod by taking $k_1^2=\omega^2\mu_0\epsilon_1$ real, we will expect (23) to represent a wave propagating without attenuation, which implies that ζ_0 is real. If ζ_0 is real and $|\zeta_0|>|k_0|$, then ν_0 is pure imaginary and $H_1^{(1)}(\nu_0\rho)$ reduces to the K_1 Bessel function which decays exponentially with increasing argument. Under these conditions, (23) represents a surface wave of amplitude A, whose field distribution outside the dielectric rod is an exponential decay. The wave propagates in the positive z direction according to $e^{-i(\omega t-\zeta_0 z)}$. The poles of the integrand are those values of ζ which cause the denominator of (22) to vanish. Equating the denominator of (22) to zero yields

$$(\nu_1 b)\frac{J_0(\nu_1 b)}{J_1(\nu_1 b)}=\epsilon_r(\nu_0 b)\frac{H_0^{(1)}(\nu_0 b)}{H_1^{(1)}(\nu_0 b)}. \tag{24}$$

For convenience of notation, let $X_1=\nu_1 b$ and $X_0=\nu_0 b$; then (24) may be written

$$X_1\frac{J_0(X_1)}{J_1(X_1)}=\epsilon_r X_0\frac{H_0^{(1)}(X_0)}{H_1^{(1)}(X_0)}. \tag{25}$$

It can be shown that the only values of real ζ for which (25) can be satisfied are for ζ in the range $|k_0|<|\zeta|<|k_1|$.[10] Recalling that $\nu_1=\sqrt{k_1^2-\zeta^2}$ and $\nu_0=\sqrt{k_0^2-\zeta^2}$, where $k_1^2>k_0^2>0$, consider ζ real and $|k_0|<|\zeta|<|k_1|$. Then ν_1 is real and ν_0 is pure imaginary. It follows that X_1 is real and X_0 is pure imaginary. Let $X_0=i\xi$, where ξ is positive real. Eq. (25) becomes

$$-X_1\frac{J_0(X_1)}{J_1(X_1)}=\epsilon_r(-i\xi)\frac{H_0^{(1)}(i\xi)}{H_1^{(1)}(i\xi)}=\epsilon_r\xi\frac{K_0(\xi)}{K_1(\xi)} \tag{26}$$

where the K_n functions are modified Bessel functions of the second kind.

A graph of the functions $-X_1[J_0(X_1)/J_1(X_1)]$ and $\epsilon_r\xi[K_0(\xi)/K_1(\xi)]$ is presented in Fig. 3. The function $-X_1[J_0(X_1)/J_1(X_1)]$ is discontinuous each time $J_1(X_1)$ vanishes and so an infinity of branches occur for ever increasing X_1. It passes through zero each time $J_0(X_1)$

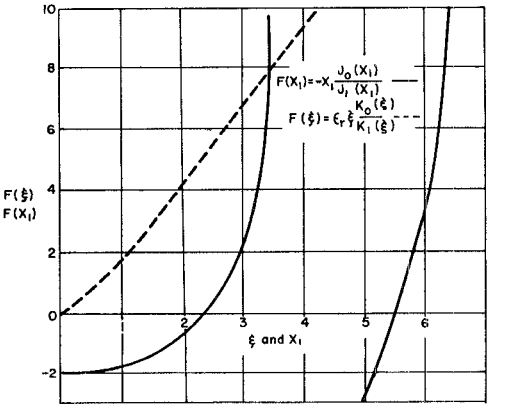

Fig. 3—Graph of the functions $F(X_1)$ and $F(\xi)$. The transcendental mode equation is $F(X_1)=F(\xi)$.

has a zero. The function $\epsilon_r\xi[K_0(\xi)/K_1(\xi)]$ approaches zero as $\xi\to 0$ and increases positively for increasing ξ. It is evident in Fig. 3 that for every finite ξ, an infinity of values X_1 exist which satisfy (26). In order to obtain a finite number of unique solutions of the mode equation, a second relation between X_1 and ξ is needed. It follows from the definitions that

$$\nu_1^2=k_1^2-\zeta^2$$
$$\nu_0^2=k_0^2-\zeta^2$$

where ζ is identically the same in ν_1 and ν_0. Elimination of ζ^2 yields

$$\nu_1^2-\nu_0^2=k_1^2-k_0^2=\left(\frac{2\pi}{\lambda_0}\right)^2(\epsilon_r-1)$$

[10] J. W. Duncan, "The Efficiency of Excitation of a Surface Wave on a Dielectric Cylinder," Antenna Lab., Elec. Eng. Res. Lab., Eng. Exper. Station, University of Illinois, Urbana, Ill., Tech. Rep. No. 32, pp. 20–22; May, 1958.

where λ_0 is the free space wavelength corresponding to the source frequency. Multiplying by b^2 yields

$$(\nu_1 b)^2 - (\nu_0 b)^2 = X_1^2 - X_0^2 = \left(\frac{2\pi b}{\lambda_0}\right)^2 (\epsilon_r - 1).$$

Since $X_0 = i\xi$, we obtain the second relation between X_1 and ξ, which is

$$X_1^2 + \xi^2 = R^2 \tag{27}$$

where

$$R = \left(\frac{2\pi b}{\lambda_0}\right)\sqrt{\epsilon_r - 1} = k_0 b\sqrt{\epsilon_r - 1}.$$

The graphical solution of (26) is illustrated in Fig. 4, which includes curves of X_1 as a function of ξ obtained from Fig. 3, and the relation (27). Note that (27) is the equation of a circle of radius R with center at the origin. The multiple solutions X_1 for every ξ as discussed with Fig. 3 are evident in Fig. 4. The first branch of X_1 starts at $X_1 = 2.405$ for $\xi = 0$ and approaches $X_1 = 3.83$ asymptotically with increasing ξ. $X_1 = 2.405$ is the first zero of $J_0(X_1)$ and $X_1 = 3.83$ is the first zero of $J_1(X_1)$. The second branch commences at 5.52 and approaches 7.02, which corresponds to the second zeros of $J_0(X_1)$ and $J_1(X_1)$, respectively. An infinity of branches is thus established.

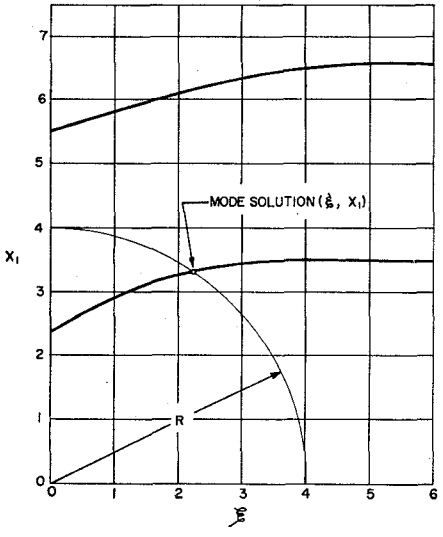

Fig. 4—Solution of the mode equation: X_1 as a function of ξ which satisfies $F(X_1) = F(\xi)$, and the relation $X_1^2 + \xi^2 = R^2$.

Consider the case $R < 2.405$. Since $X_1 = \sqrt{R^2 - \xi^2} < R$, Fig. 3 shows that (26) cannot be satisfied for $X_1 < 2.405$, that is, no solution of the mode equation exists for $R < 2.405$. This is also evident in Fig. 4. Physically, this means that the dielectric rod waveguide is below cutoff and cannot propagate a surface wave of the transverse magnetic type.

Referring to Fig. 4, if $2.405 < R < 5.52$, a single, unique solution (ξ, X_1) of (26) and (27) results. Thus, (22) has poles at $\zeta = \pm\zeta_0$, where ζ_0 may be determined from the solution (ξ, X_1). The poles occur on the real axis in the region $|k_0| < |\zeta| < |k_1|$. We see that when R is restricted to the range $2.405 < R < 5.52$, the dielectric rod propagates a single surface wave which is the lowest order, circularly symmetric, transverse magnetic mode. It is known as the E_{01} mode and propagates as $e^{i\zeta_0 z}$ for $z > 0$ and $e^{-i\zeta_0 z}$ for $z < 0$.

Solution of the Mode Equation

Specific solutions of (26) and (27) are required in order to calculate the power in the surface wave and excitation efficiency. A value of 2.56 was chosen for ϵ_r, the relative dielectric constant of the rod. R was restricted to the range $2.405 < R < 5.52$. Eqs. (26) and (27) were solved by numerical methods on the University of Illinois digital computer.[11] Six solutions (ξ, X_1) were obtained for selected values of $k_0 b$ equal to 2.2, 2.6, 3.0, 3.4, 3.8, and 4.2.

Table I presents ξ, X_1, and the ratio λ_g/λ_0 corresponding to each value of $k_0 b$. λ_g is the guide wavelength of the surface wave mode. The ratio λ_g/λ_0 follows from the definition of ν_0.

$$\frac{\lambda_g}{\lambda_0} = \frac{1}{\sqrt{1 + \left(\frac{\xi}{k_0 b}\right)^2}}. \tag{28}$$

TABLE I

$k_0 b$	ξ	X_1	λ_g/λ_0
2.2	0.5603	2.6901	0.9691
2.6	1.2329	3.0043	0.9036
3.0	1.9353	3.2086	0.8403
3.4	2.6269	3.3366	0.7913
3.8	3.2905	3.4204	0.7560
4.2	3.9264	3.4788	0.7305

Evaluation of the Contour Integral

We evaluate the integral solution (22) by considering it as a contour integral in the complex ζ plane. For convenience we write (22) in the form

$$H_\phi(\rho, z) = \int_{-\infty}^{+\infty} U(\zeta)\, d\zeta \tag{29}$$

where

$$U(\zeta) = \frac{i\omega\epsilon_1 a}{2\pi} \frac{J_1(\nu_1 a) H_1^{(1)}(\nu_0 \rho) e^{i\zeta z}}{(\nu_1 b) J_0(\nu_1 b) H_1^{(1)}(\nu_0 b) - \epsilon_r (\nu_0 b) J_1(\nu_1 b) H_0^{(1)}(\nu_0 b)}$$

$$\nu_1 = \sqrt{k_1^2 - \zeta^2}$$

$$\nu_0 = \sqrt{k_0^2 - \zeta^2}.$$

To obtain (29) we select the closed contour shown in Fig. 2, which consists of the real axis from $-R$ to $+R$, the circular arc R_1 of radius R, the path Γ along the

[11] J. W. Duncan, *op. cit.*, pp. 83–105.

branch cut and imaginary axis, and the arc R_2. Applying Cauchy's residue theorem, we write

$$\int_{-R}^{+R} U(\zeta)d\zeta + \int_{R_1} + \int_{\Gamma} + \int_{R_2} = 2\pi i \text{ Residue } U(\zeta)\Big|_{\zeta_0}. \quad (30)$$

In the limit as $R\to\infty$, the integrand $U(\zeta)$ vanishes along R_1 and R_2 so that (30) becomes

$$H_\phi(\rho, z) = \int_{-\infty}^{+\infty} U(\zeta)d\zeta = 2\pi i \text{ Residue } U(\zeta)\Big|_{\zeta_0} - \int_{\Gamma} U(\zeta)d\zeta. \quad (31)$$

The residue term of (31) is the surface wave field while the integration along Γ yields the radiation field. Evaluation of the line integral along Γ is extremely difficult. It is sufficient for our purposes to obtain an approximation to the far zone radiation field. Under these conditions the coordinates ρ and z in $U(\zeta)$ are relatively large and the integral is of the type which may be evaluated by the saddle point method of integration.[12] Instead of integrating along the path Γ we deform Γ into the path of steepest descent C_s which passes through the saddle point of the integrand. The path C_s, which is directed in the reverse sense to Γ, is shown in Fig. 2. Thus, (31) may be replaced by

$$H_\phi(\rho, z) = 2\pi i \text{ Residue } U(\zeta)\Big|_{\zeta_0} + \int_{C_s} U(\zeta)d\zeta \quad (32)$$

which is the desired form of the solution $H_\phi(\rho, z)$ in region II.

The Radiation Field

We shall now evaluate the integral $\int_{C_s} U(\zeta)d\zeta$ by means of the saddle point method of integration. In applying this method it is convenient to introduce the transformation of variable

$$\zeta = k_0 \sin\tau \quad (33)$$

where

$$\tau = \psi + i\eta.$$

Now $\tau = \sin^{-1}(\zeta/k_0)$ is a multiple-valued function of ζ and the region of integration in the ζ plane transforms into a strip in the τ plane which is bound by two curved lines corresponding to the branch cuts in the ζ plane. They are defined by

$$\sin\psi \cosh\eta = \pm 1. \quad (34)$$

The path of integration along the real axis in the ζ plane transforms to the path C_1 in the τ plane as shown in Fig. 5. The branch points $\zeta = \pm k_0$ transform to the points $\tau = \pm\pi/2$ while the images of the poles $\pm\zeta_0$ are the points $\tau_0 = \pi/2 - i\cosh^{-1}(\zeta_0/k_0)$ and $\tau_0 = -\pi/2 + i\cosh^{-1}(\zeta_0/k_0)$. The transformation (33) yields

$$\nu_0 = + k_0\cos\tau$$
$$\nu_1 = + k_0\sqrt{\epsilon_r - \sin^2\tau} = k_0 w \quad (35)$$

where for convenience we let w, a function of τ, represent the radical $\sqrt{\epsilon_r - \sin^2\tau}$. Substituting (33) and (35) into the integral $\int_{C_s} U(\zeta)d\zeta$, one obtains

$$H_\phi(\rho, z) = \frac{i\omega\epsilon_1 a}{2\pi b}\int_{C_s} \frac{J_1(k_0 aw)H_1^{(1)}(k_0\rho\cos\tau)e^{ik_0 z\sin\tau}\cos\tau d\tau}{wJ_0(k_0 bw)H_1^{(1)}(k_0 b\cos\tau) - \epsilon_r\cos\tau J_1(k_0 bw)H_0^{(1)}(k_0 b\cos\tau)}. \quad (36)$$

If ρ is large and $k_0\rho\cos\tau \neq 0$, the Hankel function in the numerator of (36) may be replaced by its asymptotic representation. Furthermore, it is convenient to introduce the spherical coordinate system shown in Fig. 6, where the polar angle θ is measured from the plane $z=0$. In this coordinate system we note that $\rho = r\cos\theta$ and $z = r\sin\theta$. Substituting for ρ and z in (36) and replacing the Hankel function by its asymptotic formula yields

$$H_\phi(r, \theta) = \frac{i\omega\epsilon_1 a}{2\pi b} e^{-i(3\pi/4)}\int_{C_s} F(\tau)\left[\frac{2\cos\tau}{\pi k_0 r\cos\theta}\right]^{1/2} e^{ik_0 r\cos(\tau-\theta)}d\tau \quad (37)$$

where

$$F(\tau) = \frac{J_1(k_0 aw)}{wJ_0(k_0 bw)H_1^{(1)}(k_0 b\cos\tau) - \epsilon_r\cos\tau J_1(k_0 bw)H_0^{(1)}(k_0 b\cos\tau)}.$$

Integral (37) is valid for r large and $k_0 r\cos\theta \neq 0$. It is readily evaluated by the saddle point method. The saddle point is defined by the equation

$$\frac{d}{d\tau}\cos(\tau - \theta) = 0 \quad (38)$$

which yields

$$\tau = \theta. \quad (39)$$

Note that the saddle point corresponds to the polar angle θ. In the ζ plane the saddle point is

$$\zeta_s = k_0\sin\theta. \quad (40)$$

[12] E. T. Copson, "Theory of Functions of a Complex Variable," Oxford University Press, London, Eng., pp. 330–331; 1955.

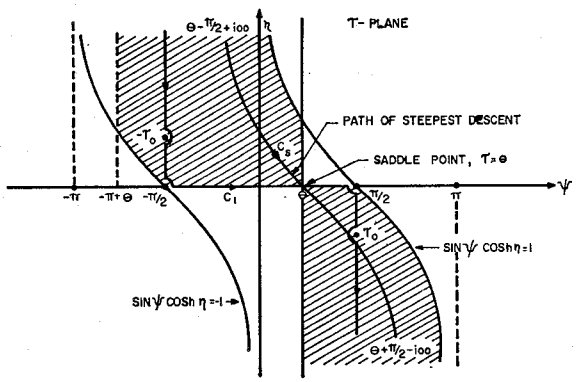

Fig. 5—Path of integration in the τ plane.

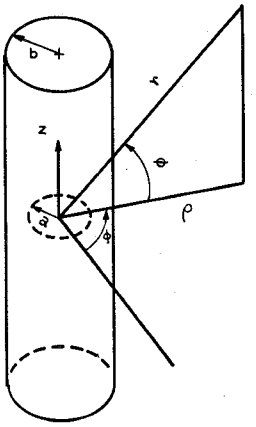

Fig. 6—Cylindrical coordinate system (ρ, ϕ, z) and spherical coordinate system (r, ϕ, θ).

The path of steepest descent C_s in the τ plane is defined by the equation

$$\sin(\psi + \pi/2 - \theta)\cosh\eta = 1. \tag{41}$$

The shaded area of Fig. 5 is the region of convergence of the integral (37) as η approaches $\pm\infty$ on C_s.

Carrying out the evaluation of (37), one obtains

$$H_\phi(r, \theta) = -i\sqrt{\frac{\epsilon_0}{\mu_0}}\left(\frac{\epsilon_r a}{\pi b}\right)F(\theta)\frac{e^{ik_0 r}}{r} \tag{42}$$

where

$$F(\theta) = \frac{J_1(k_0 aw)}{wJ_0(k_0 bw)H_1^{(1)}(k_0 b\cos\theta) - \epsilon_r\cos\theta J_1(k_0 bw)H_0^{(1)}(k_0 b\cos\theta)}.$$

It follows from Maxwell's equations that

$$E_\theta(r, \theta) = -i\left(\frac{\epsilon_r a}{\pi b}\right)F(\theta)\frac{e^{ik_0 r}}{r}. \tag{43}$$

The Surface Wave Field

Let $H_\phi^{II}(\rho, z)$ represent the surface wave field in region II. It is given by

$$H_\phi^{II}(\rho, z) = 2\pi i \text{ Residue } U(\zeta)\big|_{\zeta_0} \tag{44}$$

where

$$\rho \geq b, \qquad z > 0.$$

The pole ζ_0 is a simple pole since the denominator of $U(\zeta)$ vanishes at ζ_0 but its first derivative does not.

Carrying out the evaluation of (44), one obtains

$$H_\phi^{II}(\rho, z) = A_{II}K_1(\xi\rho/b)e^{i\zeta_0 z} \tag{45}$$

where

$$A_{II} = \frac{\omega\epsilon_1\left(\frac{a}{b}\right)J_1\left(\frac{k_0 a}{k_0 b}X_1\right)}{\zeta_0 b\left\{\frac{2(R/\xi)^2}{X_1}J_0(X_1)K_1(\xi) + \left[\epsilon_r\left(\frac{\xi}{X_1}\right) + \left(\frac{X_1}{\xi}\right)\right]J_0(X_1)K_0(\xi) + (\epsilon_r - 1)J_1(X_1)K_1(\xi)\right\}}$$

$$\zeta_0 b = \sqrt{(k_0 b)^2 + \xi^2}$$

$$R^2 = X_1^2 + \xi^2.$$

The other surface wave components in Regions I and II follow from Maxwell's equations. They are

$$E_\rho^{II}(\rho, z) = \left(\frac{\zeta_0}{\omega\epsilon_0}\right)H_\phi^{II}(\rho, z)$$

$$H_\phi^{I}(\rho, z) = A_{II}\frac{K_1(\xi)}{J_1(X_1)}J_1(X_1\rho/b)e^{i\zeta_0 z}.$$

$$E_\rho^{I}(\rho, z) = \left(\frac{\zeta_0}{\omega\epsilon_1}\right)H_\phi^{I}(\rho, z). \tag{46}$$

THE POWER INTEGRALS AND EXCITATION EFFICIENCY

The radiated power W^R is obtained by integrating the average Poynting vector over the surface of a large sphere of radius r. The radiation field, which has components E_θ and H_ϕ, is independent of ϕ and is symmetrical about the plane $\theta = 0$. The integral for the radiated power is

$$W^R = \sqrt{\frac{\epsilon_0}{\mu_0}}\left(\frac{\epsilon_r a}{b}\right)^2\frac{1}{\pi/2}\int_0^{\pi/2}\cos\theta\,|F(\theta)|^2 d\theta \tag{47}$$

where $F(\theta)$ is defined in (42).

A discussion of the integrand of (47) is worthwhile at this point. We note that the magnitude of the radiation

field is proportional to $|F(\theta)|$. As θ approaches $\pi/2$, $F(\theta)$ vanishes so the radiation pattern has a null along the axis of the dielectric rod. The influence of the source dimension (k_0a) on the radiation field and W^R is contained in the function $J_1(k_0aw)$ which is the numerator of $F(\theta)$. The dielectric rod parameter (k_0b) appears only in the denominator. In order to obtain maximum excitation efficiency for any k_0b, W^R should be a minimum. W^R will be a minimum if $J_1(k_0aw)$ vanishes or is quite small as θ ranges from zero to $\pi/2$; this occurs when $J_1(k_0aw)$ passes through a zero. Consider the function $w=\sqrt{\epsilon_r-\sin^2\theta}$ with $\epsilon_r=2.56$. As θ takes on values $0\leq\theta\leq\pi/2$, w has the range $1.25\leq w\leq 1.6$. Assume an average value for w, $w_{av}=1.42$. We should expect the most efficient source to have the approximate dimension $k_0a=3.83/w_{av}=2.7$, where 3.83 is the first zero of the J_1 function. This analysis is verified in the efficiency curves presented in the latter part of this section.

The integral (47) was evaluated numerically on the University of Illinois digital computer. W^R was computed as k_0a varied in discrete increments of 0.2 over the range $0<k_0a\leq k_0b$ for a particular value of k_0b. The results of these computations appear in the efficiency curves.

The surface wave power W^S is obtained by integrating the average Poynting vector over the surface of an infinite transverse plane normal to the z axis. Since the surface field components E_ρ and H_ϕ are different for regions I and II, separate integrations are necessary for the regions $0\leq\rho\leq b$ and $\rho\geq b$. The resulting expression for the total surface wave power is

$$W^S=\sqrt{\frac{\epsilon_0}{\mu_0}}\left(\frac{\epsilon_r a}{b}\right)^2 N^S \tag{48}$$

where

$$N^S=\pi\frac{\lambda_g}{\lambda_0}\frac{\left\{\frac{1}{\epsilon_r}\left[\frac{K_1(\xi)}{J_1(X_1)}\right]^2\left[J_0^2(X_1)+J_1^2(X_1)-\frac{2}{X_1}J_0(X_1)J_1(X_1)\right]+\left[K_0^2(\xi)-K_1^2(\xi)+\frac{2}{\xi}K_0(\xi)K_1(\xi)\right]\right\}}{\left\{2\left[\frac{\left(\frac{X_1}{\xi}\right)^2+1}{X_1}\right]J_0(X_1)K_1(\xi)+\left[\epsilon_r\left(\frac{\xi}{X_1}\right)+\left(\frac{X_1}{\xi}\right)\right]J_0(X_1)K_0(\xi)+(\epsilon_r-1)J_1(X_1)K_1(\xi)\right\}^2}J_1^2\left(\frac{k_0a}{k_0b}X_1\right).$$

Inspection of N^S shows that the source dimension (k_0a) appears only in the argument of $J_1^2[(k_0a/k_0b)X_1]$. The remaining portion, which is rather formidable, is a function of ϵ_r and the mode solution (ξ, X_1). It has a constant value for any ϵ_r and k_0b. N^S is a function of the source only by the term $J_1^2[(k_0a/k_0b)X_1]$. It should be noted, however, that a/b appears in the constant which multiplies N^S to give W^S. Selecting a value of k_0b with $\epsilon_r=2.56$, W^S was calculated according to (48) as a function of k_0a using values of λ_g/λ_0, ξ, and X_1 from Table I.

Excitation Efficiency

The efficiency with which the source delivers power to the surface wave is called the excitation efficiency of the source. Denoting efficiency by the symbol Υ, it is defined as

$$\Upsilon=\frac{W^S}{W^T} \tag{49}$$

where W^S is the surface wave power.

W^T is the total power delivered by the source.

Goubau[13] has proved that, for lossless surface waveguides, the radiation and surface wave fields are orthogonal with regard to power considerations. In this case, the total energy delivered by the source is equal to the sum of the surface wave power and the radiated power. Since we are considering a lossless dielectric rod, the orthogonality condition holds and Υ is given by

$$\Upsilon=\frac{W^S}{W^S+W^R} \tag{50}$$

where W^S is the surface wave power and W^R is the radiated power.

Efficiency was calculated according to (50) using computed values of W^S and W^R. Figs. 7 and 8 present curves of efficiency as a function of k_0a for the selected values of k_0b. Efficiencies greater than 90 per cent are predicted for k_0a approximately equal to 2.6.

Experimental Investigation

The magnetic current ring was purposely chosen for the theoretical problem because it is a source which has a simple physical realization. Consider Fig. 1. By symmetry the magnetic current filament generates a field which has no electric component in the plane $z=0$. In the plane of the source the only non-zero component of $\overline{E}$ is E_z, which is normal to the plane. Since tangential $\overline{E}$ vanishes over the plane, an infinitely large metal sheet may be placed at the source position without disturbing the field. One may simulate the source by a very narrow annular slot in a large conducting sheet or ground plane. Then, of course, the dielectric rod extends from the ground plane in only one direction. The annular slot may be illuminated using a circular or coaxial waveguide exciter. If the rod is terminated in a resistance card load which produces negligible reflection of the surface wave, then the finite rod excited by an annular slot in a ground plane simulates in a half space the theoretical problem of Fig. 1.

In order for the slot to be a good approximation of the filament, the slot width must be small compared to the wavelength and the electric field in the slot must be radial and uniform about the circumference. It is as-

[13] G. Goubau, "On the excitation of surface waves," Proc. IRE, vol. 40, pp. 865–868; July, 1952.

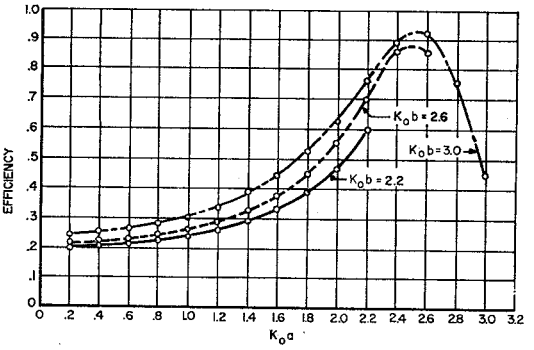

Fig. 7—Excitation efficiency as a function of the source dimension k_0a.

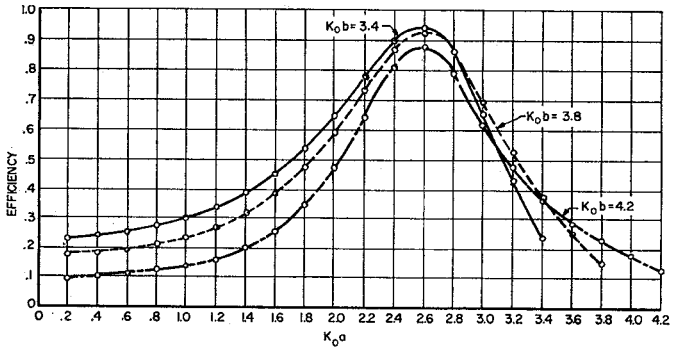

Fig. 8—Excitation efficiency as a function of the source dimension k_0a.

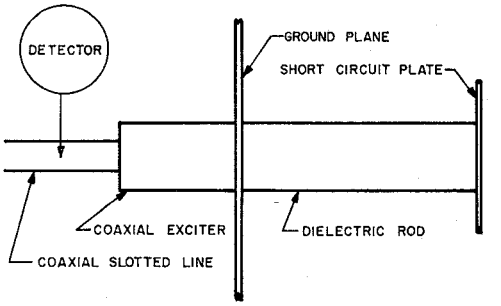

Fig. 9—Representation of the two-port junction.

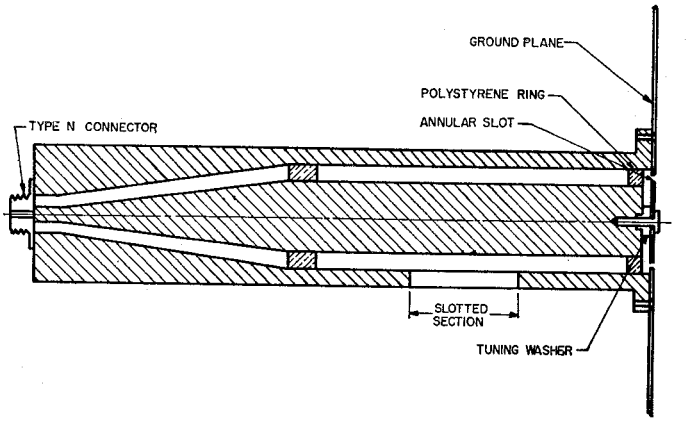

Fig. 10—Cross section of the coaxial exciter.

sumed that the mean radius of the slot corresponds to the radius of the infinitesimal current filament. The slot may be illuminated from a circular waveguide propagating the TM_{01} mode, or from a coaxial line excited in the usual TEM mode. The coaxial line is preferable since the center conductor provides a convenient means of supporting the circular disc which is the ground plane within the annular slot.

The efficiency with which the slot excites the surface wave may be measured using Deschamps' method for determining the insertion loss of a waveguide junction.[14,15] The transition from the coaxial line to the dielectric rod waveguide is considered as a two-port waveguide junction. Assuming that the dielectric rod and coaxial line are lossless, then the dissipative attenuation of the junction results entirely from the power radiated into space by the slot. If all of the power delivered to the slot is converted to the surface wave, then no power is lost as stray radiation and the junction is 100 per cent efficient. This method has been used previously to measure the launching efficiency of sources placed on a dielectric image line.[16]

A schematic representation of the arrangement used to measure the efficiency of the junction is given in Fig. 9. The measurements were performed using a 2-inch diameter polystyrene rod mounted vertically on a 60-inch square ground plane. For most of the measurements the dielectric rod was 40 cm long, although in some instances, the length was increased to 134 cm.

Using Deschamps' method, one obtains the efficiency of the entire transition between the input reference plane and the output reference plane, that is, between the measuring probe and the short circuit termination. Since we are interested in measuring the dissipative attenuation of just the annular slot, it is essential that the rest of the transition shall introduce only negligible attenuation. For the present we shall ignore the dielectric rod loss since it is very small. It follows, then, that a low loss exciter must be constructed to illuminate the annular slot. The annular slot presents a very low conductance and capacitive susceptance to the exciting waveguide. Therefore, the feed waveguide must be a low impedance line with some means of tuning out the capacitive susceptance of the slot at the ground plane position.

Fig. 10 shows a cross sectional view of the low impedance coaxial line which was constructed for this purpose. The inner diameter of the outer wall of the coax was $1\frac{7}{8}$ inches and the inner conductor diameter was $1\frac{1}{4}$ inches, which yields a 24-ohm line. A two wavelength tapered section transformed the 24-ohm line to a standard 50 ohm, type N connector. Two polystyrene

[14] G. A. Deschamps, "Determination of reflection coefficients and insertion loss of a waveguide junction," *J. Appl. Phys.*, vol. 24, pp. 1046–1050; August, 1953.

[15] H. F. Mathis, "Experimental procedures for determining the efficiency of four-terminal networks," *J. Appl. Phys.*, vol. 25, pp. 982–986; August, 1954.

[16] R. H. DuHamel and J. W. Duncan, "Launching efficiency of wires and slots for a dielectric rod waveguide," TRANS. IRE, vol. MTT-6, pp. 277–284; July, 1958.

rings centered the inner conductor within the cylinder. The ring at the ground plane position was a quarter-wavelength transformer which would match the 24-ohm line to a 9.5-ohm resistance load. A circular tuning disc or washer was placed on the end of the center conductor to provide a series inductive reactance to cancel the capacitive susceptance of the slot. The circular disc which formed the inner boundary of the annular slot was fixed to the tuning washer and the coax center conductor by a special mounting screw. Since the neighborhood of the annular slot and tuning washer is a resonant cavity, all parts were silver-plated to minimize losses.

A family of discs and rings were fabricated to permit varying the annular slot radius from $\frac{1}{2}$–$\frac{7}{8}$ inch while maintaining the slot width constant at $\frac{1}{8}$ inch. The $\frac{1}{8}$ inch slot width corresponds to .067 λ_0 and .076 λ_0 at k_0b equal to 3.4 and 3.8, respectively. Recalling that the radius of the dielectric rod is 1 inch, it is convenient to express the slot radius in the normalized form a/b; then the source dimension k_0a for any k_0b is given by $k_0b(a/b)$. Six slots were constructed for the measurements. Table II gives the normalized slot radius a/b, and the corresponding dimension k_0a at the two values of k_0b which were used for the measurements.

TABLE II

Normalized Slot Radius a/b	k_0a When $k_0b=3.4$	k_0a When $k_0b=3.8$
0.50	1.70	1.90
0.625	2.12	2.38
0.687	2.34	2.61
0.75	2.55	2.85
0.812	2.76	3.08
0.875	2.98	3.32

A slot $\frac{1}{8}$ inch wide and 2 inches long was milled in the side wall of the exciter so that the standing wave ratio in the exciter could be measured. After a particular slot was mounted on the exciter, various tuning washers were tested until one was found which reduced the VSWR in the exciter to less than 2 when the dielectric rod was terminated with a matched load. The image circle was determined from measurements made in a coaxial slotted line which was connected directly to the exciter through a type N elbow connector.

When efficiency was measured as shown in Fig. 9, the result obtained was not precisely the excitation efficiency of the annular slot; instead it was the efficiency of the entire transition between the measuring probe and the short circuit termination. Although the losses in the system were small, the measured efficiency was reduced somewhat by the dielectric rod attenuation and by the loss between the measuring probe and the ground plane. The system losses were measured approximately by means of Deschamps' method.[17] The measurements of slot launching efficiency were then corrected to account for the system losses.

[17] Duncan, *op. cit.*, pp. 66–72.

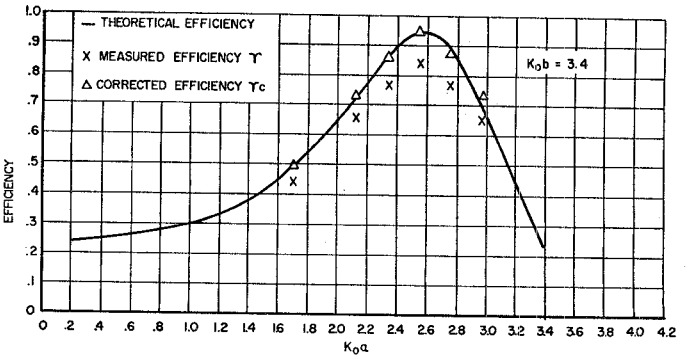

Fig. 11—Comparison of the theoretical and measured excitation efficiency.

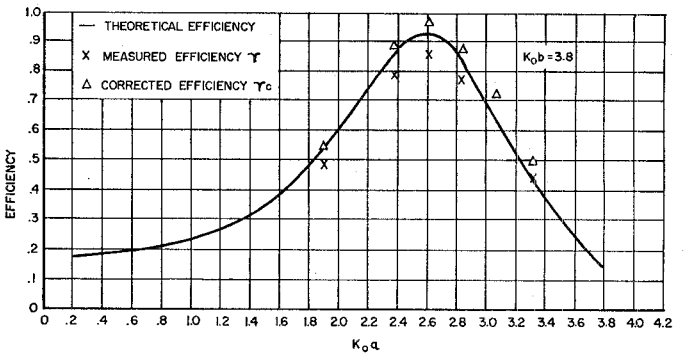

Fig. 12—Comparison of the theoretical and measured excitation efficiency.

Six slots were measured in the laboratory. Measurements were performed at frequencies of 6387 mc and 7138 mc which result in k_0b equal to 3.4 and 3.8, respectively. The results are presented in Figs. 11 and 12 for comparison with the theoretical curves of efficiency. The data include the measured efficiency Υ and the corrected efficiency Υ_c for each source k_0a. The very close agreement between the experimental points and the theoretical curve is evident. In all cases the measured efficiency Υ, which *included* the system losses, was within 10 per cent of the efficiency predicted by theory. The experimental measurements verify that an excitation efficiency of approximately 95 per cent may be obtained from an annular slot of dimension $k_0a=2.6$.

It should be emphasized that a good "matched" transition is necessary in order to realize the high efficiency of the annular slot. In the laboratory the predicted source efficiencies were not measured until the matched transition of the coaxial exciter was constructed. Of course, the efficiency of the annular slot is independent of the feed structure, but substantial coupling of power from the closed waveguide to the surface waveguide is obtained only when a good impedance match is provided at the aperture plane. Otherwise, a very high standing wave ratio exists in the vicinity of the aperture and most of the power delivered by the feed waveguide is reflected.

As a point of practical interest, the efficiency of the annular slot in the presence of a small ground plane was

determined. This effect was investigated by measuring slot efficiencies as the size of the ground plane was reduced. Surprisingly, the ground plane dimension had little effect on the efficiency. At least, this was the case at the two values of k_0b which were considered. The ground plane was reduced to a 10-inch diameter flange and no appreciable change in efficiency was noted. Consequently, the ground plane was removed so that the launching structure consisted of the dielectric rod mounted on the coaxial exciter. Efficiency was measured at k_0b equal to 3.4 and 3.8. The results are presented in Table III which includes, for comparison, the efficiency that was measured *with* the large ground plane. Note that these data have not been corrected to account for the system losses.

TABLE III

k_0b	k_0a	Efficiency With Ground Plane	Efficiency No Ground Plane
3.4	1.70	0.44	0.428
	2.12	0.65	0.647
	2.34	0.76	0.779
	2.55	0.835	0.847
	2.76	0.77	0.829
↓	2.98	0.65	0.696
3.8	1.90	0.48	0.545
	2.38	0.775	0.776
	2.61	0.85	0.835
	2.85	0.77	0.776
	3.08	0.63	0.63
↓	3.32	0.44	0.413

Acknowledgment

The author wishes to thank Prof. V. H. Rumsey who was his adviser at the beginning of the research and Dr. E. C. Jordan who was his adviser at its conclusion. He is indebted to Dr. R. H. DuHamel for several helpful suggestions and is particularly grateful to Dr. P. E. Mayes of the University of Illinois Antenna Laboratory for his counsel throughout the entire work.

The help of G. Berryman and K. Rosenberg, who performed most of the experimental measurements and numerical computations, is sincerely appreciated.

Proposal for a Tunable Millimeter Wave Molecular Oscillator and Amplifier*

J. R. SINGER†

Summary—**An atomic beam apparatus suitable for a millimeter wave generator is theoretically discussed. The beam consists of atoms having a net magnetic moment. The upper and lower Zeeman levels of the atomic beam in a magnetic field are spatially separated by an inhomogeneous magnetic field. The upper state atoms enter a cavity where transitions occur at a frequency determined by a static magnetic field. The resonant frequency of the cavity is set at the transition frequency. The positive feedback of the cavity allows operation as an oscillator. Some of the more important parameters for oscillator operation are evaluated. The upper frequency limit is determined primarily by the resonant structure design.**

Introduction

THE ammonia gas maser invented by Gordon, Zeiger and Townes[1] shows considerable promise as a frequency standard and as a narrow band amplifier. One limitation is the fixed frequency operation which is determined by the natural transition frequencies of the NH_3 molecule. An extension of the molecular beam technique which permits operation of a molecular oscillator amplifier in the mm wave region with a power output of the order of the ammonia maser is suggested in this paper.

The present scheme uses a Stern-Gerlach[2] type of molecular beam arrangement for achieving a polarized beam of atoms. The atoms in the lower energy state may be readily removed from the beam since they are spatially separated. The upper state atoms then adiabatically enter a homogeneous magnetic field region where they are subjected to an RF field polarized in the appropriate direction to induce atomic transitions. Induced transitions are always coherent in phase and amplification of RF is achieved if the rate of transitions times the energy from each transition exceeds the RF power input and the system losses. The system may be used as an oscillator since spontaneous emission will induce further transitions by use of a high Q structure

* Manuscript received by the PGMTT, September 30, 1958; revised manuscript received, December 8, 1958. This work was supported by the Faculty Res. Com., University of California, and the U. S. Air Force under Contract No. AF 49(638)-102 monitored by the A. F. Office of Sci. Res., Air Res. and Dev. Command.

† Electronics Res. Lab., Univ. California, Berkeley, Calif.

[1] J. P. Gordon, H. J. Zeiger and C. H. Townes, "The maser," *Phys. Rev.*, vol. 99, pp. 1264–1274; August 15, 1955.

[2] W. Gerlach and O. Stern, "Der Experimentelle Nachweiss des Magnetischen Moments des Silberatoms," *Zeit. Physik*, vol. 8, pp. 110–112; December, 1921.